Terra Antartica Reports
2000, **4**, 241-258

Relationship among X-Ray Lithofacies, Magnetic Susceptibility, P-Wave Velocity and Bulk Density in Core ANTA95-89C (Ross Sea, Antarctica): First Results

R. Bonaccorsi[1], A. Brambati[1], M. Busetti[2] & G.P. Fanzutti[1]

[1]Dip. Scienze Geologiche, Ambientali e Marine, Università di Trieste, Via Weiss 2, 34127 Trieste - Italia
[2]Ist. Nazionale di Oceanografia e Geofisica Sperimentale, Borgo Grotta Gigante 42/c, 34010 Sgonico (Trieste) - Italia

**Corresponding author* (bonaccor@univ.trieste.it)

INTRODUCTION

Sedimentary facies from continental margins contain records of depositional processes within the outer shelf-slope system during different climate phases. Physical properties measurements are commonly used to track changes in ice rafted sediment (Niessen et al., 1998, Nishimura et al., 1998), for non-invasive analyses of whole sedimentary cores and between-core correlation (Pudsey & Camerlenghi, 1989).

Because some Antarctic continental marginal sequences are often condensed (Domack & Harris, 1998), and only a few outer slope cores from the Ross Sea were investigated (Leventer & Stevens, 1996), there is a basic need to develop ultra-high resolution procedures in order to identify the best sampling strategy. In fact, complex and condensed internal structures, such as those inferred by X-ray observation of core ANTA95-89C, may be easily overlooked with a visual examination. In general, if the distinction between laminates and massive lithofacies is clear, the sedimentary model of similar types of diamicton and/or laminations remains vague and difficult to interpret. This is particularly true when marine laminated sediments are genetically related to outer slope glacial sedimentary environments characterized by complex deep-sea processes. Because of this, ANTA95-89C presents an opportunity to test the resolution of these methods. Secondly, preliminary results will be useful for future in-depth study of this core, and may provide insights into cryogenic sedimentation in the Ross Sea during glacial-interglacial transitions.

Cores from the Pacific margin of the Antarctic Peninsula contain lenticular laminations which were interpreted as hemipelagites to muddy contourites deposited under weak variable energy flow pulses (Pudsey & Camerlenghi, 1998). Fine sub-mm size lamination were interpreted as real marine varves characterized by high sedimentation rates of up to 2.5 m/kyr (Grobe et al., 1992). While reports of laminated lithofacies from the Antarctic peninsula were available and date back to 1970's (Leventer & Stevens, 1996), information on laminated sediments from the Ross Sea are scarce and scattered through the literature (Nishimura et al., 1998; Brambati et al., 1997).

Only a limited number of works described laminated mud from the Ross Sea (Leventer et al., 1993), and the major findings were only briefly reported (Leventer & Stevens, 1996). Silty mm-size laminations from the continental slope were described and interpreted as seasonal successions

of biogenic (*i.e.*, single layers of different diatom species) and lithogenic flux (Leventer & Stevens, 1996). In another study, low magnetic susceptibility (MS) muddy layers interbedded with higher MS silty laminations were described from core GC1606 (northern Ross Island, inner Glomar Challenger basin) and related to an under-floating-ice shelf environment present during the LGM (Nishimura et al., 1998).

X-ray phothograps offer an advantage in the easy identification of massive lithofacies. However, relevant differences occur between primary diamicton, directly deposited by ice shelves (ISRD) on the continental shelf, and secondary diamicton, represented by Iceberg Rafted debris (IBRD) (Kellogg & Kellogg, 1989). Thin, high-density packed, and low to high-density structureless massive diamictons are potentially related to episodic fallout of IBRD, especially when alternating with laminated layers (Pudsey & Camerlenghi, 1998).

A fine to coarse-grained stratified diamicton unit, described as "laminated" was recognized by X-ray photographs in ANTA-91 30C (Drygalski Basin). The unit boundaries were dated between 18.1 and 10.9 kyr BP, and cold-dense water flow was likely responsible for its layered structure (Brambati et al., 1997). Structureless massive, low to high-density diamicton with sparse chaotic gravel is a lithofacies which is produced in seaward sub-ice shelf environments (Domack & Harris, 1998), sediment drift (Pudsey & Camerlenghi, 1998), and is found in deep-sea cores from both northern and southern hemispheres. Domack & Harris (1998) recognized a very similar X-ray condensed lithology in cores collected in the central north side of the Ross Sea Embayment and in the Mac Robertson Shelf. In these cores, massive and laminated lithofacies alternate.

Relevant points of interest, which will be addressed in further investigations, are whether the different isolated massive layers shared similar genetic mechanisms, depositional process and sources. Studies of this nature have not yet been carried out in the Southern Ocean as they have for the North Atlantic, due to lack of geological information from the Antarctic continent.

In the North Atlantic, multi-component investigation via radiogenic isotopes, demonstrated that a) the composition of sand-size-IRD (*i.e.*, different ratios of biogenic carbonatic debris and terrigenous inputs) can be due to different sources and pathways, and b) differences and similarities can occur between the glacial and interglacial background sediment (*sensu* Gwiadza et al. 1996), which contain the coarse IRD. In fact, the lead isotopic composition patterns, within the same Heinrich layer 3 (H3), differs between the western North Atlantic sites (*e.g.*, core V28-82). Also, Heinrich layers H6 and H3 (Gwiadza et al., 1996), and H1 (Hemming et al., 1998) from V28-82 have significant geochemical and lithostratigraphic differences relative to H2, H4, and H5.

Comparisons of physical parameters (*i.e.*, P-wave velocity vs. Magnetic Susceptibility) can detect compositional differences (*i.e.*, dilution of carbonate-bearing sediments by IBRD) and dropstones lithology (*e.g.*, granite, dolerite clast) (Niessen & Jarrad 1998). Niessen & Jarrad (1998) suggested the use of "empirical relationship" between physical parameters in the framework of Cape Roberts Project (CRP-1). In this paper we will investigate whether there is a similar empirical relationship between physical properties of ANTA95-89C. We will attempt to identify differences between the coarse IRD fraction, background sediment, and laminated facies. Then, we plan to test if the variables affecting the r values of the empirical relationships can be identified (*i.e.*, by sediment and multi-component radiogenic isotopes analyses), and whether physical properties patterns can provide investigators with a valuable diagnostic tool for tracking differences in ultra-high mode. Finally, we will use these relationships to validate first-hand information on deep processes in the outer slope sedimentary environment, and investigate how the Ross Sea Antarctic margin responded to past climate change.

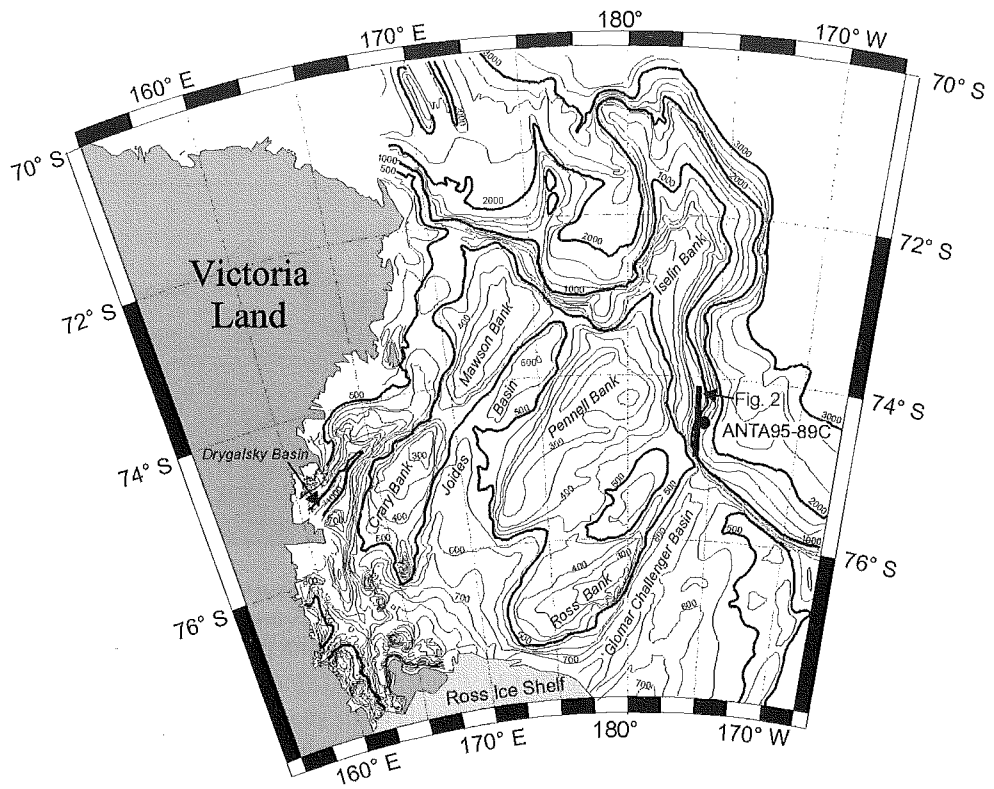

Fig. 1 - Bathymetry of the Western Central Ross Sea. The map shows the location of core ANTA95-89C. Solid lines represent the isobaths at 500, 1000, 2000 and 3000 m-depth.

STUDY AREA

ANTA95-89C, a 404 cm-long gravity core, was taken from the outer slope of the Ross Sea (74 29.100'S – 175 34.059'W) at a water depth of 2058 m (Fig. 1) during the 1994/95 austral summer cruise of the *R/V Italica* (PNRA). The core was collected from the lateral gentle slope (rise environment) close to the main canyon drainage system along the same Glomar Challenger Basin orientation (Fig. 1). The basin morphology is genetically related to Ice Stream "C" activity (Bentley & Jezek, 1981) and the confluence of Ice streams A and B (Anderson et al., 1992; Hughes, 1977). Deep-sea processes in the northeastern side of the Ross Sea remain poorly understood and only a limited number of deep-sea cores, mainly collected during *Eltanin* cruises, were examined (Anderson et al., 1992; Osterman & Kellogg, 1979; Truesdale & Kellogg, 1979; Watkins, 1972). A complex channel-levee system was recognized from analysis of seismic data in this part of the outer slope (Fig. 2). Hence, the geological setting of the area, and its special bottom topography might potentially lead to a variety of oceanographic and sedimentary processes (*e.g.*, high density flows related to advances and retreats of the ice shelf, turbidity events, contourite flows, etc.). Consistent submarine erosion (Fillon, 1972) was recognized by the occurrence of mixed middle Tertiary to early Quaternary diatom assemblages (Truesdale & Kellogg, 1979).

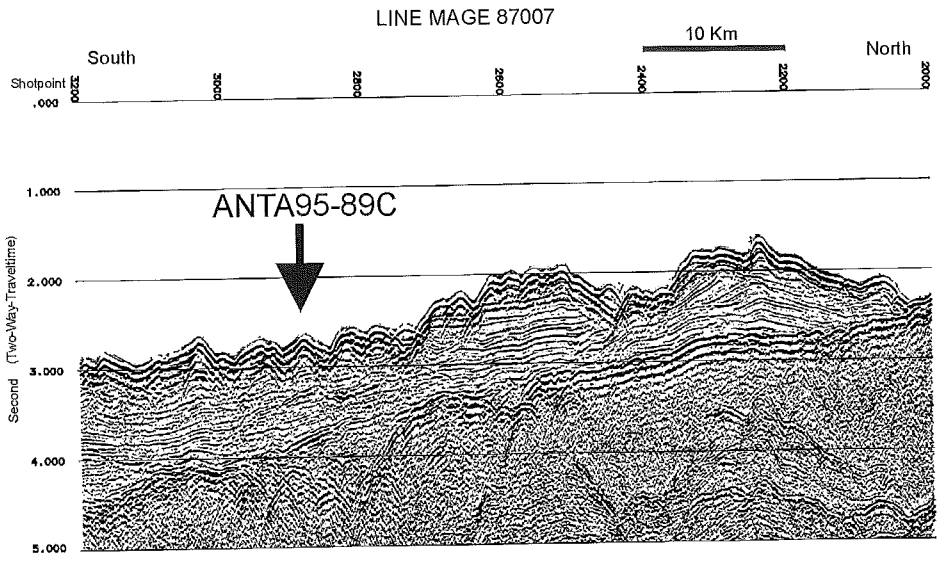

Fig. 2 - Multi-channel seismic line M87007 (SCAR Antarctic Seismic Data Library System) collected during the 1987 Marine Geological Expedition (MAGE) of Murmansk (Russia). Core ANTA95-89C was taken 2-km away from the profile. The Core is positioned on the seismic transect to show its location relative to the channel-levee systems area (See Fig. 1 for location).

Benthic foraminiferal assemblages of recent species were also recognized from sites proximal to the study area (Osterman & Kellogg, 1979) perhaps related to Pleistocene sediments (Truesdale & Kellogg, 1979).

MATERIALS AND METHODS

By assuming that the single levels characterized by pure end-member lithofacies represent discrete sedimentary episodes, several different methods were used to identify them. They consisted of *i*) preliminary identification of the main lithofacies by X-ray photographs; *ii*) estimation of the physical properties logs and covariation in order to identify different intervals and down-core trends; *iii*) comparison of the detected boundaries from the previous two steps to constrain the best sedimentary intervals; *iv*) quantification of each interval physical features using statistical parameters such as Average and Standard Deviation (STD), the lowest STD representing pure physically well characterized end-members lithofacies; *v*) to further test the end-member lithofacies by Correlation Coefficient (r) and identify potential changes in the sources and processes building up apparently similar sedimentary sequences.

X-RAY PHOTOGRAPHS –ANALYSIS AND LITHOFACIES IDENTIFICATION

X-ray photographs (Agfa Strutturix DX 4) were made at the "Grandi Motori" facility in Trieste, and a total of ten negative 40 cm-long radiographs were analyzed. The textural composition of sedimentary intervals was interpreted by gray-tone pattern from the sediment responses to the X-rays penetration and any fine to coarse structure of the matrix (*i.e.*, muddy, sandy, tephra layers, wavy lamination, IRD-gravel pattern, etc.) can be easily detected (Bouma, 1964; Backer &

Tab. 1 - X-ray color standard determination proposed for X-ray lithofacies according to the Munsell Soil Color Chart (1975) (gray scale for gley-type sediemnt). One or more features, listed in column (on the right), are interpretations from X-ray lithofacies and intervals.

Munsell Soil Colour Chart code	*Colour name*	*X-ray lithofacies*	*Intervals*	*Interpretation*
5B 7/1	ligth bluish gray	L2a, D3, SD2	INT-1, INT-2b, INT-5b, INT-12a, c	- bioturbated mud - sandy laminations - pebbles/cobbles - single lamina - high density IRD
5B 6.5/1	Light bluish- bluish gray	D3, SD1, SD2	INT-4, INT-8, INT-10, INT-12b, INT-16	- low density IRD - mud chips - IRD - tiny-layer
5B 6/1	bluish gray	L3	INT-17, INT-18	- fine silty-sand sediment - homogenous mud
5B 5.5/1	bluish gray	L2b	INT-3	- mud veins and inclusions - fine laminated sandy mud
5B 5/1	bluish gray	L1	INT-7a, 7c, INT-9b	- homogenous mud
5B 4.5/1	Bluish-dark-bluish-gray	L1, L2	INT-19, INT-22, INT-13	- sub-mm laminated mud - single cm-thick mud lamina
5B 4/1	Dark bluish gray	L2	INT-11	- cm/mm-thick laminated mud

Friedman, 1969). The gray-tone pattern of each X-ray photograph was quantified by using the Gray scale of the Munsell Soil Color Chart (1975) for Gley soil-type (HUE 5B) in order to provide a standard descriptive tool. Four main "VALUE" degrees (from 7/1 to 4/1) and the same "CHROMA" (/1) allowed any slight change in the color of the X-ray photographs to be described at least by seven degrees of color (Tab. 1) as they result from a combination of all possible intermediate values (*i.e.*, 6.5/, 5.5/, and 4.5/). This procedure provides a standard chromatic description for different X-ray lithofacies (Tab. 1).

PHYSICAL PROPERTIES MEASUREMENTS

Logs of physical properties were acquired by the Multi Sensor Core Logger (MSCL Geotek Ltd., UK), a non-destructive automated system that can log Wet Bulk Density (WBD), P-Wave Velocity (Vp), and Volume Magnetic Susceptibility (VMS). 1-cm sampling was used. The technical specification are summarized elsewhere (Gunn & Best, 1998; Niessen et al., 1998). The density log acquiring procedure employs a radioactive source of ^{137}Cs emitting a 1.0-cm gamma ray beam crossing the core liner each 20 s-measurement. The conversion from gamma ray absorption to WBD is based upon parameters obtained by experimental calibration. The P-Wave Velocity measurement system consists of two transducers. The transmitter generates a 250 kHz short P-wave pulse detected by the receiver after it propagates through the core. The travel distance is measured from the external core diameter, and a temperature correction is required to process the P-wave velocity raw data (Gunn & Best, 1998; Niessen et al, 1998).

Two Volume MS data sets were both collected by using a Bartington loop sensor having 3-cm horizontal resolution. The first whole-core Magnetic Susceptibility (VMS-1) measurement was acquired by using a 2-cm interval sensor during the R/V *Italica* cruise. The second one (VMS-2) was acquired together with other physical properties at 1-cm intervals via MSCL. The two measurements were made to test if different sampling conditions (*i.e.*, different operators, sensor resolution, and onboard/land based data acquisition), and a three-year core storage time will affect the results.

Tab. 2 - Average and STD calculated for the Volume and Mass Susceptibility, P-wave Velocity, P-wave Amplitude, and Wet Bulk Density for Unit A and B, and the 41 intervals. L1, L2, L3, and SD1, SD2, D3 are the main laminated/massive lithofacies to which the main Intervals 1 to 32 belong. Further explanation in the main text and Core key.

Interval	MSCL-Interval	N°	Volume SM (SI)	N°	Mass MS (SI) cm³ g-1	N°	Vp (m/s)	N°	P W Amplitude	N°	WBD g/cm³	Lithofacies Type
INT-1	0.6-9.6	10	34.9 ± 3.5	8	19.9 ± 1.7	9	1614.7 ± 15.2	10	100.0 ± 0.0	8	1.77 ± 0.03	L2
INT-2	10.6-17.6	8	27.8 ± 1.3	8	16.1 ± 0.7	8	1593.6 ± 2.9	8	100.0 ± 0.0	8	1.72 ± 0.02	L2
INT-2a	10.6-13.6	4	37.6 ± 1.7	4	21.0 ± 0.7	4	1618.0 ± 5.3	4	100.0 ± 0.0	4	1.79 ± 0.02	L2
INT-2b	14.6-16.6	3	27.0 ± 0.0	3	15.65± 0.2	3	1592.4 ± 3.0	3	100.0 ± 0.0	3	1.72 ± 0.02	SD2
INT-3	18.6-40.6	22	24.0 ± 1.8	20	14.0 ± 0.7	20	1586.5 ± 2.9	23	96.3 ± 17.3	20	1.69 ± 0.01	L2
INT-4	41.6-45.8	2	29.5 ± 0.7	0	nr	1	1579,7	6	74.2 ± 31.5	0	nr	D3
INT-5	46.8-92.8	47	32.4 ± 3.6	47	18.2 ± 1.7	47	1600.5 ± 10.5	47	99.8 ± 1.2	47	1.78 ± 0.05	L2
INT-5a	46.8-71.8	26	31.5 ± 3.0	26	18.0 ± 1.4	26	1594.0 ± 8.3	26	100.0 ± 0.0	26	1.75 ± 0.04	L2a
INT-5b	72.8-79.8	8	38.0 ± 0.8	8	20.5 ± 0.7	8	1616.9 ± 6.2	8	99.0 ± 2.8	8	1.85 ± 0.03	L2b
INT-5c	80.8-92.8	13	30.6 ± 2.4	13	17.2 ± 1.3	13	1601.9 ± 2.5	13	100.0 ± 0.0	13	1.79 ± 0.02	L2a
INT-6	93.8-110.8	18	20.9 ± 3.7	18	12.0 ± 2.1	18	1612.3 ± 7.0	18	100.0 ± 0.0	18	1.75 ± 0.02	L2
INT-7	111.8-127.8	17	23.6 ± 3.3	17	13.4 ± 1.9	17	1628.6 ± 5.5	17	100.0 ± 0.0	17	1.75 ± 0.01	L1, L2
INT-7a	110.8-115.8	6	22.8 ± 0.4	6	13.0 ± 0.2	6	1623.7 ± 3.6	6	100.0 ± 0.0	6	1.76 ± 0.01	L1
INT-7b	116.8-119.8	4	21.8 ± 0.5	4	12.4 ± 0.3	4	1628.8 ± 2.9	4	100.0 ± 0.0	4	1.76 ± 0.01	L2
INT-7c	120.8-126.8	7	23.6 ± 2.2	7	13.4 ± 1.3	7	1631.3 ± 4.8	7	100.0 ± 0.0	7	1.75 ± 0.01	L1
INT-8	128.8-138.8	11	68.6 ± 11.8	11	36.5 ± 5.3	11	1653.9 ± 13.9	11	98.5 ± 3.2	11	1.87 ± 0.06	D3
INT-9	139.8-187.0	48	31.0 ± 8.2	29	19.8 ± 4.4	29	1613.9 ± 8.5	48	64.5 ± 41.2	29	1.78 ± 0.02	L1, L2
INT-9a	139.8-158.8	20	35.1 ± 10.6	14	22.1 ± 5.2	14	1621.2 ± 3.7	14	77.1 ± 37.9	14	1.79 ± 0.03	L2
INT-9b	159.8-172.0	13	24.7 ± 1.7	29	nr	-	nr	-	nr	-	nr	L1
INT-9c	173.0-187.0	15	31.0 ± 3.0	15	17.6 ± 1.7	15	1607.1 ± 5.3	15	91.5 ± 18.7	15	1.77 ± 0.01	L2
INT-10	188.0-195.0	8	42.3 ± 6.5	8	23.0 ± 3.0	8	1623.5 ± 17.6	8	88.5 ± 16.2	8	1.83 ± 0.08	D3
INT-11	196.0-213.0	18	24.4 ± 4.0	18	14.0 ± 2.3	18	1617.6 ± 5.0	18	100.0 ± 0.0	18	1.74 ± 0.01	L2
INT-12	217.0-238.0	22	149.8 ± 55.9	22	73.9 ± 29.2	22	1742.9 ± 122.2	22	69.5 ± 27.2	22	2.04 ± 0.09	D3
INT-12a	217.0-222.0	6	217.8 ± 36.8	6	109,7 ± 19.0	6	1653.0 ± 32.4	6	42.3 ± 32.1	6	1.99 ± 0.02	D3
INT-12b	223.0-228.0	6	161.5 ± 34.6	6	80.0 ± 17.7	6	1751.1 ± 144.6	6	84.2 ± 16.0	6	2.02 ± 0.06	D3
INT-12c	229.0-237.0	9	105.0 ± 7.9	9	19.8 ± 3.8	9	1805.3 ± 119.6	9	74.4 ± 16.9	9	2.11 ± 0.09	D3
INT-13	239.0-261.0	23	37.8 ± 6.7	23	19.0 ± 3.1	23	1683.6 ± 18.8	23	100.0 ± 0.2	23	1.98 ± 0.04	L2
INT-14	262.0-266.0	5	47.8 ± 1.9	5	23.0 ± 0.9	5	1742.3 ± 15.2	5	100.0 ± 0.0	5	2.08 ± 0.04	D3
INT-15	267.0-282.0	16	40.5 ± 2.8	15	19.9 ± 1.1	15	1716.4 ± 25.1	16	99.3 ± 2.8	15	2.03 ± 0.04	L2
INT-16	283.0-292.2	10	49.7 ± 6.9	5	26.4, ± 1.0	6	1719.5 ± 6.8	10	80.9 ± 36.8	5	2.11 ± 0.03	D3
INT-17	293.2-298.2	6	54.8 ± 2.9	6	26.4 ± 1.4	6	1715.9 ± 7.1	6	100.0 ± 0.0	6	2.08 ± 0.01	L3
INT-18	299.2-309.2	11	67.2 ± 3.2	11	32.1 ± 1.6	11	1738.3 ± 60.7	11	99.0 ± 3.3	11	2.09 ± 0.02	SD1
INT-19	310.2-314.2	5	62.0 ± 3.7	5	30.5 ± 1.2	5	1669.1 ± 13.1	5	100.0 ± 0.0	5	2.03 ± 0.05	L2
INT-20	314.2-319.2	6	72.0 ± 2.3	6	34.2 ± 1.3	6	1709.0 ± 13.1	6	100.0 ± 0.0	6	2.11 ± 0.03	SD1
INT-21	320.2-328.2	9	73.0 ± 0.5	9	34.4 ± 0.4	9	1695.7 ± 10.7	9	100.0 ± 0.0	9	2.07 ± 0.02	L3
INT-22	329.2-336.2	8	75.8 ± 4.0	8	35.9 ± 1.7	8	1722.0 ± 14.5	8	100.0 ± 0.0	8	2.11 ± 0.02	D3
INT-23	337.2-343.2	7	73.7 ± 3.1	7	35.1 ± 1.3	7	1732.5 ± 3.5	7	99.0 ± 2.6	7	2.10 ± 0.01	SD1
INT-24	344.2-346.2	3	77.3 ± 0.6	3	36.9 ± 0.5	3	1715.0 ± 12.3	3	100.0 ± 0.0	3	2.10 ± 0.02	L2
INT-25	347.2-349.2	3	79.7 ± 1.2	3	37,9 ± 0.9	3	1723.6 ± 9.1	3	100.0 ± 0.0	3	2.10 ± 0.02	D3
INT-26	350.2-353.2	4	77.0 ± 0.8	4	36.7 ± 0.5	4	1725.2 ± 3.6	4	100.0 ± 0.0	4	2.10 ± 0.01	SD1
INT-27	354.2-357.2	4	77.8 ± 0.5	4	36.9 ± 0.5	4	1732.4 ± 8.3	4	100.0 ± 0.0	4	2.11 ± 0.03	SD2
INT-28	358.2-364.2	7	79.0 ± 1.0	7	37.4 ± 0.6	7	1734.4 ± 10.0	7	100.0 ± 0.0	7	2.11 ± 0.02	L3
INT-29	365.2-380.2	16	70.7 ± 3.3	16	33.7 ± 1.5	16	1737.0 ± 5.0	16	100.0 ± 0.0	16	2.09 ± 0.02	D3
INT-30	381.2-385.2	5	82.2 ± 4.3	5	38.7 ± 1.6	5	1772.5 ± 20.4	5	100.0 ± 0.0	5	2.12 ± 0.03	L2
INT-31	386.2-396.2	11	94.1 ± 4.0	11	43.6 ± 1.9	11	1008.1 ± 7.4	11	100.0 ± 0.0	11	2.16 ± 0.01	SD2
INT-32	397.2-404.2	3	92.3 ± 0.6	3	42.3 ± 0.2	8	1791.9 ± 41.7	8	99.3 ± 2.1	7	2.16 ± 0.03	D3
Unit-A	0-216	212	31.6 ± 12.6	187	18.2 ± 7.0	189	1611.0 ± 18.4	212	90.5 ± 25.4	187	1.76 ± 0.05	L1, L2, SD2, D3
Unit-B (*)	238-404	162	63.8 ± 18.2	156	30.9 ± 8.1	162	1727.3 ± 40.3	167	98.6 ± 10.0	160	2.08 ± 0.06	L3, SD1, SD3, D3
Unit-B (**)	217-404	183	74.1 ± 37.9	177	36.3 ± 19.0	183	1729.2 ± 56.4	188	95.2 ± 16.1	181	2.08 ± 0.06	L3, SD1, SD3, D3

Notes: IRD-1 = high density, IRD-2 = low density, IRD-3 = stratified

PHYSICAL PROPERTIES AND X-RAY PHOTOGRAPHS

The X-ray lithology was compared with the two Volume Magnetic Susceptibility data sets (VMS-1 and VMS-2), Mass Susceptibility (calculated from VMS-2), Wet Bulk Density (g/cm^3), Vp (cm/s), and P-wave Amplitude (non-dimensional) logs. Details of the expanded physical logs coupled with the X-ray photographs (Figs. 5 a, b, and c) illustrate how the high-resolution patterns can detect changes in the complex sequences of the alternating lithofacies. The selected levels from procedure *i* to *iv* were considered for calculation of Average, Standard Deviation (Tab. 2) and Correlation Coefficient ($-1<r<1$). For each of the 41 intervals (Tab. 3) **r** was calculated among Vp, WBD and Mass MS by assuming that any sensitive variation of **r** might track at least changes in the processes shaping the sedimentary model of each layer.

Tab. 3 - Correlation Coefficient (**r**) calculated for a) Mass S.M vs. WBD, b) Mass S.M vs. Vp, and c) Vp vs. WBD for the same intervals of Tab. 2. Both the **r** values for some minor (*i.e.*, 12a, 12b and 12c) and main intervals (i.e., 2, 5, 7, 9 and 12) are provided to demonstrate that they increase their significance (**r** between 0.8 and 0.9 and sometimes near 1) when calculated for high resolved end-member lithofacies. The "MSCL-Interval" column indicates the discrete interval containing the core logger data (points of counting) used for calculations.

INTERVAL	Lithofacies	Interval	MSCL-Interval	Vp vs. WBD	Vp vs. MS	MS vs. WBD
INT-1	L2	0-10	0.6-9.6	0,954	0,948	0,783
INT-2	L2	10-17	10.6-16.6	0,563	0,124	0,433
INT-2a	L2	10-14	10.6-13.6	-0,516	-0,990	0,544
INT-2b	SD2	15-17	14.6-16.6	0,531	-0,536	-1,000
INT-3	L2c	18-41	17.6-40.6	0,436	-0,159	0,069
INT-4	SD2	41-46	41.6-45.8	n.r	n.r	n.r
INT-5	L2	46-93	46.8-92.8	0,924	0,634	0,639
INT-5a	L2	46-72	45.8-71.8	0,861	0,815	0,891
INT-5b	L2	72-80	72.8-79.8	0,692	-0,638	-0,912
INT-5c	L2	80-93	80.8-92.8	0,813	0,307	0,381
INT-6	L2	93-111	93.8-110.8	-0,359	-0,241	0,756
INT-7	L1/L2	111-127	111.8-126.8	0,218	0,598	-0,172
INT-7a	L1	111-117	110.8-166.8	0,875	0,261	0,376
INT-7b	L2	117-120	117.8-119.8	0,573	-0,596	-0,161
INT-7c	L1	120-127	120.8-126.8	-0,121	0,988	-0,148
INT-8	D3	127-139	127.8-138.8	0,904	0,879	0,979
INT-9	L2	139-187	139.8-187.8	0,544	0,750	0,665
INT-9a	L2	139-159	139.8-158.8	0,642	0,730	0,597
INT-9b	L1	159-173	159.8-173.8	n.r	nr.	n.r
INT-9c	L2	173-187	174.8-186.8	0,026	0,782	0,128
INT-10	D3	187-195	187.0-194.0	0,695	0,683	0,433
INT-11	L2	195-217	195.0-216.0	0,207	0,144	0,736
INT-12	D3	217-238	217.0-238.0	0,686	-0,395	-0,476
INT-12a	D3	217-223	217.0-222.0	0,384	0,027	-0,323
INT-12b	D3	223-228	223.0-228.0	0,577	0,850	0,641
INT-12c	D3	228-238	229.0-238.0	0,652	-0,168	0,248
INT-13	L2	238-262	239.0-262.0	0,921	0,610	0,569
INT-14	D3	262-267	263.0-267.0	0,849	0,609	0,173
INT-15	L2	267-281	268.0-281.0	0,929	0,746	0,692
INT-16	D3	281-293	281.0-293.2	0,182	-0,086	0,697
INT-17	L3	293-298	293.2-298.2	0,746	-0,903	-0,534
INT-18	SD1	298-309	299.2-309.2	-0,653	-0,342	-0,202
INT-19	L2	309-314	310.2-314.2	0,944	0,66	0,667
INT-20	SD1	314-319	315.2-319.2	0,965	-0,902	-0,853
INT-21	L3	319-328	320.2-328.2	0,877	0,751	0,732
INT-22	D3	328-336	329.2-336.2	0,674	0,286	0,543
INT-23	SD1	336-342	337.2-342.2	0,684	0,368	0,806
INT-24	L2	342-345	343.2-345.2	0,924	-0,926	-1,000
INT-25	D3	345-348	345.2-348.2	0,292	0,932	0,537
INT-26	SD1	348-351	349.2-351.2	0,071	0,882	-0,408
INT-27	SD2	351-356	352.2-356.2	0,896	0,819	0,789
INT-28	L3	356-364	357.2-364.2	0,984	-0,659	-0,685
INT-29	D3	364-380	365.2-380.2	0,534	0,097	0,289
INT-30	L2	380-384	381.2-385.2	0,995	0,999	0,991
INT-31	SD2	384-396	386.2-396.2	0,481	-0,215	-0,104
INT-32	D3	396-404	397.2-404.2	0,979	-0,345	0,916

RESULTS

ANTA95-89C consists of at least 32 main intervals with some minor intervals (a to c) within them (Figs. 3, 4 and 5). A total of 41 intervals originate from the downcore alternation of six laminated and massive lithofacies types. Two Units, A and B, are present. Unit A includes Intervals 1 (a high 10-cm bioturbated top) to 11 (a Low density laminated mud), while Unit B (217-404 cm-depth) includes Intervals 12 to 32 (Fig. 3).

In the following description high/low density (H-D/L-D) terminology is related to light/dark-gray tone from X-ray photographs (Tab. 1), and, in most of the cases, really corresponds to such higher/lower Wet Bulk Density values.

Laminated (L1, L2 and L3) and massive diamicton layers including three different types of

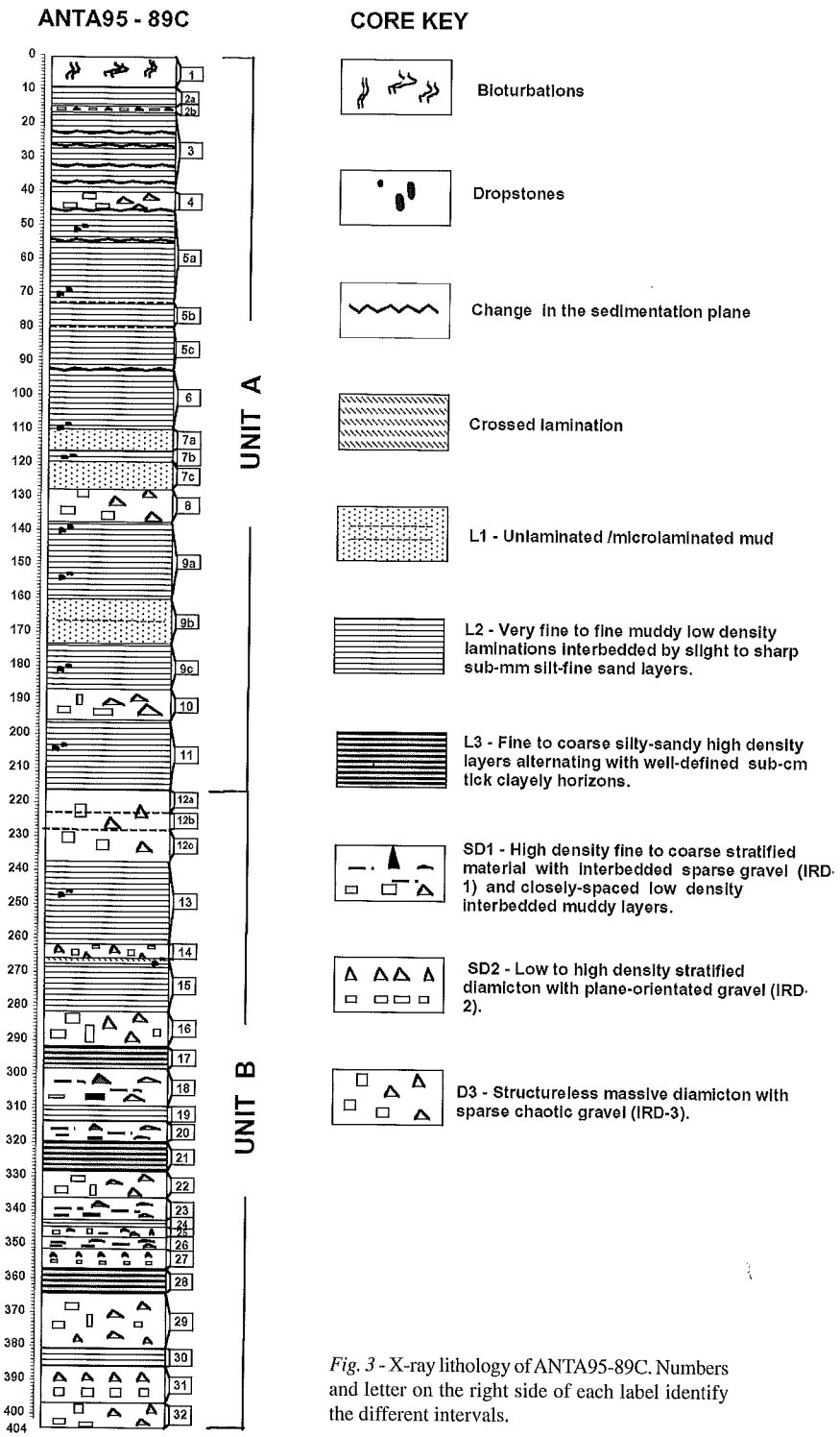

Fig. 3 - X-ray lithology of ANTA95-89C. Numbers and letter on the right side of each label identify the different intervals.

lithofacies (SD1, SD2 and D3) were categorized as follows.
Lithofacies L1 consists of non-laminated/microlaminated to weakly laminated mud. Distinctions among this lithofacies are difficult because sharp limits are often lacking. L1 was recognized only for Intervals 7a, 7c and 9b.
Lithofacies L2 mainly consists of slight to sharp sub-mm to mm high-density silt-sandy laminations (L2a) alternating with fine to coarse-grained, sub-cm to cm-thick, low-density muddy layers (L2b).
Lithofacies L3 is a fine to coarse-grained, high-density, laminated silt-sand sediment with layers somewhat closely-spaced by L-D, even well-defined, sub-cm to cm-thick clayey horizons.
Lithofacies SD1 is characterized by high density, fine to coarse-grain stratified sediment with sparse gravel (IRD-1) and closely spaced interbedded L-D muddy layers. It is very similar to L3 but includes gravel clasts.
Lithofacies SD2 is a L-D to H-D stratified diamicton with plane-orientated gravel (IRD-2).
Lithofacies D3 is a structureless massive/diamicton dominated by chaotic, clustered to sparse mm to cm-sized gravel (IRD-3) inside an H-D to L-D sandy matrix. Gravel shape and dimension can vary.

The relationship between lithofacies and intervals, as well as their absolute physical values are shown in Tables 2 and 3. In general, the very fine to fine-laminated lithofacies progressively increase in frequency and thickness to the top of the core, while the massive lithofacies, which dominate the lower section, show more condensed features (Fig. 3). Unit A includes laminated L1 and L2 alternating with four massive SD2 and D3, which correspond to Intervals 2b, 4, 8 and 10 (Figs. 3 and 4). Intervals 1 to 6 are L2 characterized by several changes in the sedimentation plane (Fig. 5a). In this unit, lithofacies L3 and SD1 are absent.

Unit B is characterized by massive SD1, SD2, D3 somewhat interbedded by L2 and L3 (Fig. 4). These laminated lithofacies progressively decrease in thickness and never exceed 9-10 cm-thickness below Interval 13 (283 cm-depth). They also seem slightly different from the laminated lithofacies of Unit A because they are denser, somewhat coarser, and have an apparent silt-sandy/silty-sand composition.

The top of Unit B, Interval 12, marks the change from Unit A. Three distinct peaks of WBD, Vp, and P-Wave Amplitude values are clearly associated with the limits of the internal Intervals 12a, 12b, and 12c (Fig. 5b). A prominent peak is also present in Volume MS (up to 250K) and in Mass MS (up to 130 χ). Unit B has thinner intervals dominated by condensed massive lithofacies characterized by lower physical property values relative to Unit A (Fig. 6). In fact, Mass MS values vary from 9.2 (Unit A) to 126.9 SI unit (Interval 12 of Unit B) with an average of 18.2 cm^3/g for Unit A and 30.9 cm^3/g for Unit B. Vp values vary from 1577 (Unit A) to 1991 (Interval 12) m/s with averages of 1,611 m/s for Unit A and 727 m/s for Unit B; BWD range from 1.67 to 2.24 (g/cm^3) with averages of 1,76 g/cm^3 for Unit A and 2.08 g/cm^3 for Unit B. Averages of Volume MS range from 31.6 (Unit A) to 63,8 (Unit B) SI. Internal peaks in WBD correspond to massive lithofacies (Intervals 8 and 10 in Unit A, and Intervals 12 to 32 in Unit B), also well matched to the other physical parameters. In Unit A, and in Interval 12 of Unit B, Volume MS peaks where isolated diamicton occurs. However, Wet Bulk Density also peaks in Interval 5a (72-80 cm), which corresponds to an extremely well-resolved sub-mm dense (silty) laminated interval. The P-Wave Amplitude, a raw, non-dimensional parameter, normally used as quality control during MSCL acquiring procedures, seems to be a diagnostic tool because it can fully track dropstones (*i.e.*, at 53, 72, 111, 117, 138, 156, 204, 248, 266-cm depth) and isolated cobbles (*i.e.*, 222, 236, 340 cm-depth) occurring within the laminated mud and coarse sandy matrix of some massive layers (Fig. 4 and Fig. 5 a, b).

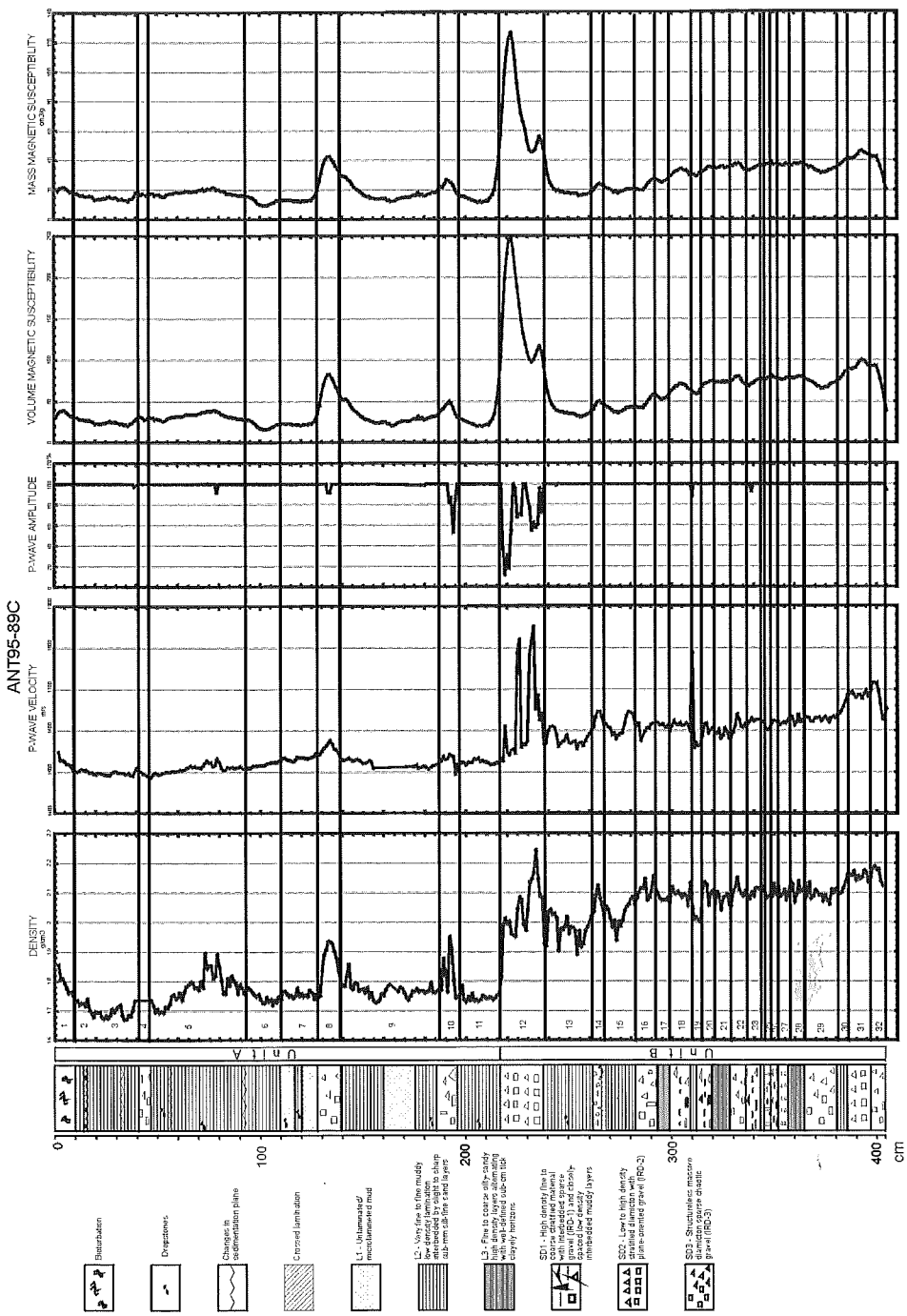

Fig. 4 - Logs of physical properties and X-ray lithology. Two main units (Unit A and Unit B) were identified according to the abrupt change of physical properties at 217-cm depth. The 32 intervals were selected by combining the X-ray radiograph analysis and physical properties correlation. (See Table 2 for numerical data).

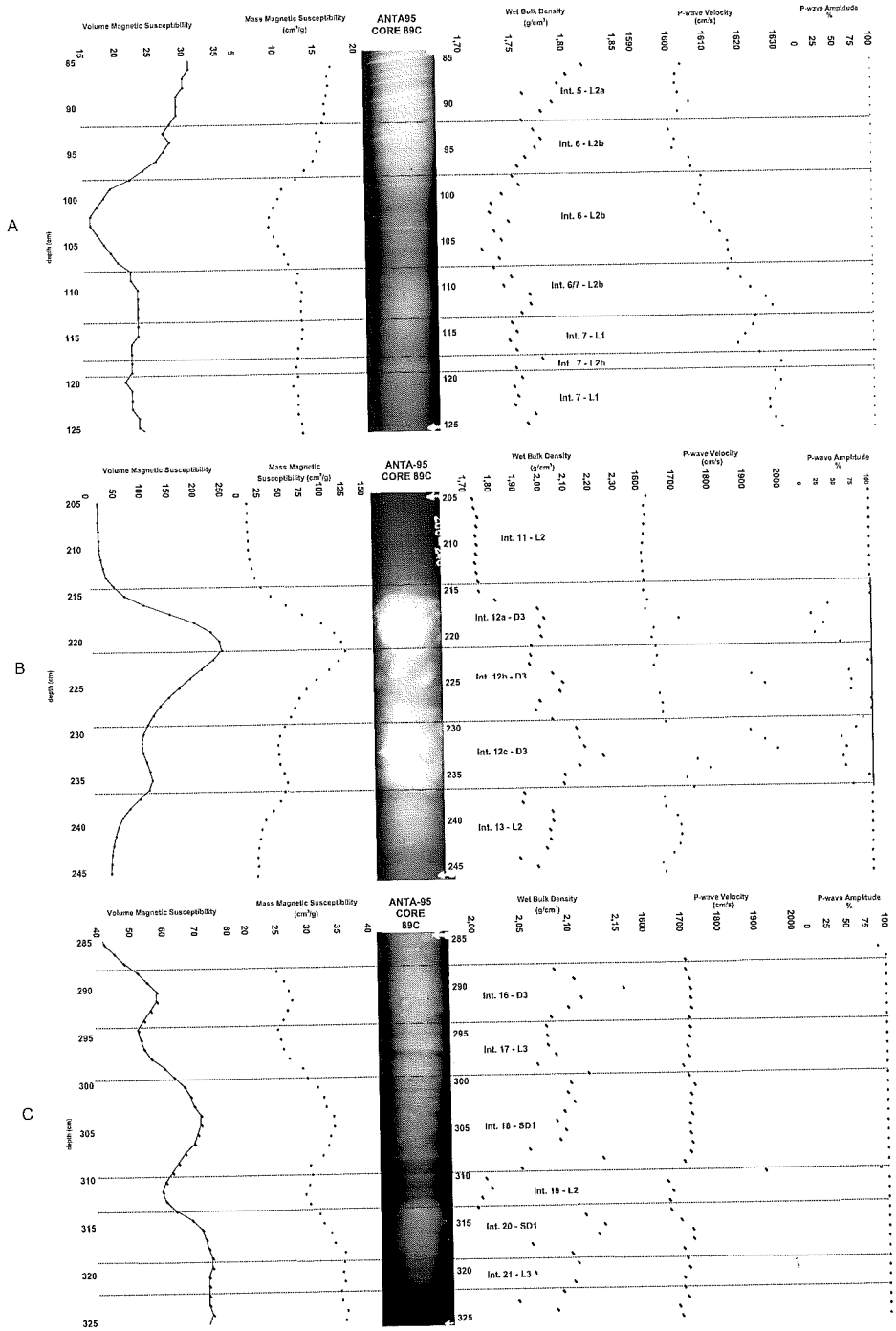

Fig. 5 - Examples of X-ray lithofacies L1, L2, L3, SD1, SD2 and D3, together with detailed logs of Volume and Mass MS-2, Wet Bulk Density (WBD), P-wave Velocity (Vp) and Amplitude (Amp.), are shown for selected intervals of core ANTA95-89C. Interval numbers and lithofacies type are shown close to each X-ray photograph. The log of P-wave amplitude illustrates the sensitivity of this parameter for detecting IRD-pebble/cobble components.

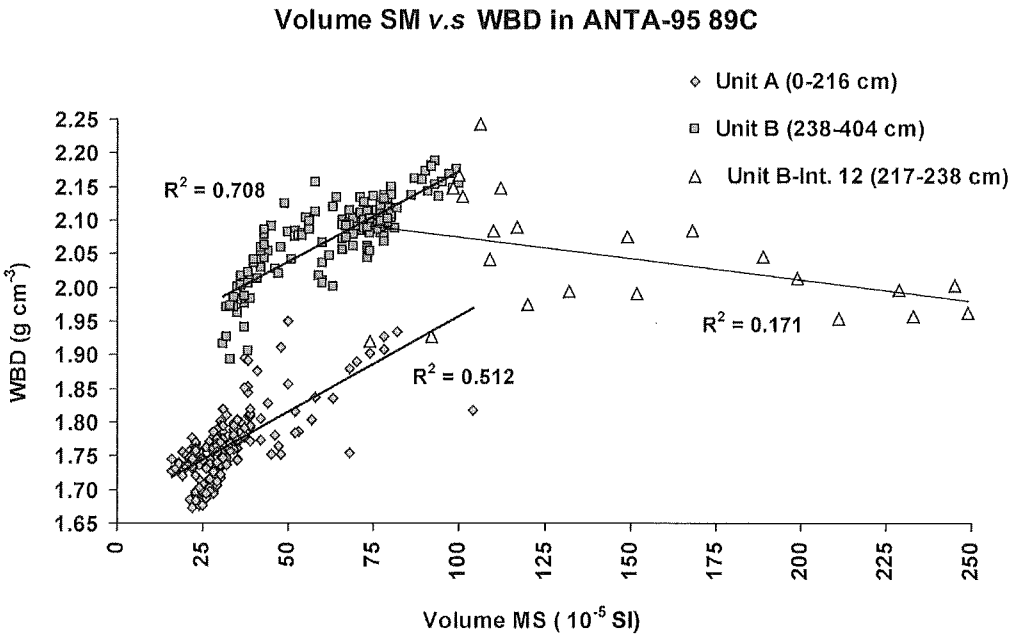

Fig. 6 - Volume Magnetic Susceptibility versus Wet Bulk Density. The two clusters, representing Unit A and Unit B are clearly defined. A separate plot of Level 12 values (included in Unit B) takes account for its quite scattered physical signature, likely related to the cobbles dimension. Note the different pattern in respect to Unit A and Unit B.

EMPIRICAL RELATIONSHIP

Correlation Coefficient (r) results are shown in table 3 (hereinafter they will be referred as empirical relationship). The three r somewhat show variable downcore values. Drastic changes in one or more values of r mark the Unit A lithostratigraphy. Intervals 2b, 8 and 10 have different values of r. In Interval 8 and 12b (and less in Interval 10) all three r-values are high positively correlated. The almost perfect negative value of r (*i.e.*, WBD *vs.* MS) makes the difference between Interval 2b and Intervals 10 and 8. Interval 12b strongly differs from Intervals 12a and 12c according to the x-ray observation, and the absolute average values of these intervals (see Tab. 2). Both Intervals 12a and 12c also have a similar r-pattern.

Unit B contains a more condensed interval sequence. It is characterized by MS *vs.* Vp and MS *vs.* WBD relationship with very high oscillating values of r, which changes from interval to interval. The empirical relationship WBD vs. Vp has a conservative pattern characterized by very high and stable r-values (*i.e.*, Intervals from 19 to 24 and Intervals from 27 to 32). Intervals 17 and 28, and in particular, Intervals 20 and 24, share the same r-signature. That is, a very high negative values (r near -1.000) for WBD vs. MS and Vp vs. MS, which are associated with a very high positive r-value for Vp vs. WBD (r greater than 0.950).

Also, intervals from 8 to 15 are mainly characterized by r>0, while intervals from 1 to 7b, from 17 to 20, and from 24 to 28 show extreme changes in r, which can pulse from high r>0 to high r<0 values. This strong oscillation affects only the relationship of Vp and WBD *vs* MS, and

implies that the condensed intervals 24 to 28 represent lithofacies with changes due to a factor affecting the Magnetic Susceptibility, and the P-wave velocity rather than the Wet Bulk Density. For instance, negative values of this empirical relationship add the information that these coarse silty-sand intervals show MS inversely correlated to Vp and WBD. Also, this interval package is constrained at its extremes by two D3 lithofacies (Fig. 3), which correspond to Intervals 22 and 29. In these intervals the empirical relationships completely change (see Tab. 2).

DISCUSSION

LITHOFACIES

Coupling X-ray analyses and physical records allows us to identify two units (Unit A and Unit B) characterized by physically well defined laminated and massive lithofacies, which are related to different absolute values (Tabs. 2 & 3). Within each unit, laminated lithofacies (L1, L2, and L3) are characterized by lower values of WBD, Vp, Volume and Mass SM, relative to the massive lithofacies (SD1, SD2, and D3). Since distinct glaciomarine environments were potentially recognizable in the whole core, it is quite important to discuss and interpret the sensitivity of the physical logs in detecting any changes related to different sedimentary processes.

A channel-levee system, and more glacial conditions, were likely responsible for the presence of the laminated lithofacies. Analyses of the processed data (*i.e.*, physical trend-lithofacies/sub lithofacies relationship, average ± STD, and changes in the downcore r values) suggest different depositional processes related to the lithofacies L1 and L2 within Unit A, and lithofacies L3 within Unit B.

Lithofacies L1 may be related to hemipelagic sedimentation during interglacials.

Lithofacies L2 is mainly associated with an average thickness near 0.5 mm. It is reasonably similar to those interpreted as real marine varves deposited under high sedimentary rate conditions (Grobe et al., 1992).

Some of the low-density L2-type laminated lithofacies may be similar to those described by Nishimura et al. (1998). Their occurrence in the inner Glomar Challenger basin was probably due to a glacial phase during which an under-ice depositional environment prevented any coarse sand–size IBRD discharge. The bottom topography of ANTA95-89C site, as well of CG1606, might account for the presence of laminated intervals. In fact, cores taken from the Joides Basin (Franklin Island) and the marginal side of Drygalski Basin (northwestern slope of Crary Bank) usually lack laminations.

The wavy laminations, well detected by peaks in all of the physical logs, seem to be related to changes in the energy of bottom currents. Several changes in the sedimentation plane (*i.e.*, at 50 and 93 cm) may be related to some erosive processes acting during the early Holocene. In fact, a strong sedimentary hiatus older than 10 800 yr BP was recognized in the topmost portion of the outer-shelf core ANTA95-77C2 (Bonaccorsi et al., this volume). This assumption is reasonable since the two cores were retrieved from the same outer shelf-to-slope pathway, along the central Eastern Ross Sea side of the Antarctic continental margin.

Sub-lithofacies L2a and L2b were emphasized within Intervals 5, 6 and 9, on the basis of *i*) their variable thickness, and *ii*) the relative dominance of fine laminated silty components within cm-thick muddy layers. It is possible that similar laminations, representing seasonal variation of lithogenic and biogenic fluxes (Leventer and Stevens, 1996), are annual varves recognized from the Ross Sea (Leventer et al., 1993). However, weak parallel mud laminations similar to L2b (*i.e.*,

Interval 11) and lenticular ones were interpreted as hemipelagites to muddy contourites deposited under weak irregular energy flow pulses (Pudsey and Camerlenghi, 1998).

Lithofacies L3 is perhaps more closely related to glacial/interglacial phases with some sporadic episodes of grounding/calving line retreat and, consequently, increase of bottom water circulation under a floating ice shelf.

Thin, high-density packed massive SD2-type lithofacies (*i.e.*, Interval 2b) and low to high-density structureless D3 are potentially related to episodic fallout of iceberg rafted debris especially when alternating with dominant laminated layers (Pudsey & Camerlenghi, 1998).

However, the presence of a laminated lithofacies similar to SD2 could be controlled by the formation of cold-dense water from East Antarctic Ice Sheet (EAIS) (Brambati et al., 1997).

Lithofacies D3 are widespread in Unit A (*i.e.*, Intervals 2b, 4, 8, and 10). Because of their razor-shaped anatomy, they look similar to Heinrich layers (H1-5) recognized in the North Atlantic (Heinrich, 1988; Andrews and Tedesco, 1992; Bond et al., 1993). However, the IRD layers from ANTA95-89C can have an opposite meaning (such as glacial vs. interglacial) due to their higher latitude environmental setting (Watkins et al., 1974; Keany et al., 1976). In fact, continental margin sites, when related to sea ice proximal zone, get very sensitive to any increase in the IRD input induced by calving line pulses. The physical analyses can track compositional differences between glacial and interglacial background sediment (*sensu* Gwiadza et al., 1996), and coarse IRD fraction can be expected within and between the different massive/stratified diamicton of core ANTA95-89C.

The alternating lithofacies detected by X-ray-photographs might be either related to late Pleistocene-Holocene (300-10 kyr up to present time), or even older events if several hiatuses were present. Also, several alternating layers between fine muddy laminated and massive sandy/pebbly sediments, as those recognized by Domack and Harris (1998), can attest to alternating phases related to advance-retreat of the ice shelf grounding/calving line system in the central north side of the Ross Sea Embayment. Indeed, some of them are perhaps related to the Last Glacial Maximum (LGM), or to another unidentified cold /warm pulse.

VOLUME AND MASS MAGNETIC SUSCEPTIBILITY

Volume MS-II vs. Volume MS-I shows a significant positive correlation ($r = 0.995$, $N=202$). Such a comparison provides an estimate of the sensitivity of the 2-cm measurement, and confirms that no changes occurred either during shipment or the three-year repository time of ANTA-89C. In fact, Magnetic Susceptibility changes can easily occur due to disturbance (Rack et al., 1995) or alteration of ferromagnetic properties because of potential biomineralization of magnetic minerals by microbial activity (Moskowitz et al., 1993). Unit A is characterized by low-density laminated levels (such as L1 and L2) corresponding to low Volume and Mass MS values (average $K<40$, average $\chi<20$), and SD3 massive-type ones with well-shaped Volume and Mass MS peaks (K up to 80, χ up to 45).

In Unit B MS shows a high frequency trend corresponding to the 10-20 cm-thick layer, and an increase of values with respect to depth. Interval 12, a diamicton including çm-sized cobbles, shows very high values (average $K=149.8$, average $\chi=73.9$). The frequency of cyclic variations increases under Interval 15 and, despite the alternating laminated and massive lithofacies, the Volume and Mass MS are not sensitive enough to distinguish clearly between them.

Biogenic sediments are usually characterized by low values of Mass MS, while high values correspond to terrigenous, clastic and/or authigenic ferromagnetic minerals such as magnetite debris (Bloemendal et al., 1992; Rack et al, 1995). Within Unit A, the well resolved lithofacies L1

and L2, alternating with sporadic SD1 and SD3 layer, might be due to a dominance of biogenic sedimentation underlying a progressive and more stable persistence of oceanic conditions. An increase of biogenic debris is expected when an ice edge retreats during an interglacial phase. In Unit B, the increase of Volume and Mass MS with depth, and the massive dominating lithofacies, are likely related to the alternating persistence of more glacial conditions, perhaps modulated by several episodes of ice shelf expansion/regression.

Ice rafted sediments, having apparently similar fabric, can be related to a wide variety of depositional environments. SD1 lithofacies from Unit A may represent IBRD that occur in a dispersed upper core pattern. SD2 seems to be related to the described stratified "compound Ice Shelf Rafted Debris" (ISRD) that indicates an Ice Shelf Zone environment (Kellogg & Kellogg, 1988).

Interval 12 has an independent trendline (Fig. 6) and its typical WBD *vs* VMS signature is consistent with a drastic change in r value related to VMS parameter (Tab. 3) and, when considered separately, the difference among Intervals 12a, 12b and 12c becomes relevant. They might contain either IRD melted out from an overlying Ice shelf, or current reworked ISRD pushed out from the shelf because an unusual number of cm-sizes clasts occurs within the diamicton matrix.

Finally, the frequently alternating downcore SD1, SD2 and D3 sequences that become quite condensed within Unit B, are likely due to such a different shift in the mode of primary and secondary glacigenic deposits according to the scheme of Kellogg & Kellogg (1989). Among these, for instance, intervals 24 to 28 could have been deposited under different sedimentary processes that the drastic changes in the empirical relationship (change in the r values) might be able to track.

PROCESSES

Potential changes in the geology of exposed interior landforms, different topographically induced pathways, and cold/warm-based glacier conditions, should be taken into account to explain the lithofacies driven by climate or shaped by local environmental conditions.

By considering that the core was recovered from the bottom of the slope, more than 2000 m-deep, in an area characterized by channel-levee system, the sediment could be genetically related to submarine gravity flow. Hence, fine and coarse facies could be related to the distance of sediment source, in this case the shelf edge. Even if the alternating laminated and massive lithofacies are both present in the two units, there is a predominance of laminated facies in Unit A, and a dominance of massive ones in Unit B. It may be that the continental shelf edge was wider during the deposition of Unit B, due to an expanded ice sheet. While retreating, the ice sheet mainly generates fine grain deposits (as those in Unit A) at the shelf edge. The alternating facies observed might testify to cyclical glacial advances and retreats. The potential hiatus between Units A and B, also emphasized by the drastic difference in WBD, marks the drastic changes between the two phases, and Unit B might be significantly older than Unit A. It is obviously impossible to distinguish between an erosive and non-depositional regime solely on the basis of X-ray observations. However, it is reasonable to argue that bottom current erosion and/or down-slope high-density flows induced the hiatus. Also, potential relationships between sea-level change and rapid decoupling of the marine ice sheet were proposed for some drastic events related to such abrupt late Pleistocene (Thomas & Bentley, 1978) to LGM glacial terminations (Grobe et al., 1992). Therefore, it is possible that the drastic alternation of lithofacies (such as the D3 at Interval 12), which occurred in Core 89C testifies to rapid disintegration of the ice sheet. It is also possible that Interval 12 doesn't represent a turbidity event because of a) the Mass SM increases up core

(perhaps due to cm-size cobbles), and b) the apparent absence of direct grading from Interval 12c through 12a (X-ray proxy).

Other important factors to take into account are the potential contribution of more ice streams and glaciers from the interior (*e.g.*, Transanctarctic Mountains, Dry Valleys) as they are potential sources of detritus contributing to the sedimentary processes (debris flow). Additionally, since lithofacies SD1, SD2 and D3 (*i.e.*, interval from 14 to 32) show sensitivity changes in their Correlation Coefficient (Tab. 3), their IRD supply might be related to different phases of the Ross Sea glacial palaeodrainage system. In fact, a different contribution from WAIS (West Antarctic Ice Sheet) and EAIS can be expected due to their different glacial dynamics over time (Oppenheimer, 1998). A similar contribution from both these sides to the Core 89C site is possible since the Glomar Challenger basin develops at the boundary between WAIS and EAIS drainage system. The different lithofacies, are in fact tuned by several primary and secondary interacting factors that affect glacial transportation, calving and glacial rafting (Warnke, 1970).

CONCLUSIONS

The comparison of two independent series of observations, such as X-ray photographs and physical property measurements, can be useful for high-resolution investigations and non-destructive analyses on cores. It provides remarkable results in identifying lithofacies lacking sharp contacts at less than 1-cm resolution. This is especially useful when these boundaries are not visible under direct observation, and/or for planning quick strategies for high-resolution sampling.

Three types of laminated (L1, L2 and L3) and massive lithofacies (SD1, SD2 and D3), were recognized by X-ray photographs in core ANTA95-89C, and these lithofacies were also well matched by the physical properties logs.

Units A and B were identified using all variations of the physical proxies, but WBD was most sensitive. Unit A is characterized by laminated L1 and L2 and sparse massive D3 lithofacies with lower average values. Unit B mainly includes massive SD1, SD2 and D3 and less laminated L3 lithofacies. Also, within each unit, laminated lithofacies show physical values lower than those measured for the massive ones.

The lithofacies analysis indicates a hiatus at 217 cm-depth between Unit A and Unit B. The dramatic change in sedimentation was probably triggered by a glacial vs. interglacial climatic and/or environmental switch. In fact, mainly massive lithofacies occurrences (and high Volume and Mass MS values) characterized the glacial phase, while the interglacial was dominated by the settling of only sparse diamicton levels within the laminated ones. L1 and L2 are probably more influenced by biogenic sedimentation because of lower values of Volume and Mass MS. The genesis of lithofacies was due to glacial/interglacial fluctuations of a variable grounded Ross Ice Shelf, glacial dynamical regimes, and deep-water processes in an outer slope environment characterized by a channel-levee system. Gravity flows can provide material removed from the shelf edge by the bulldozing action of an advancing ice sheet or from the slope itself. Additionally, bottom currents, producing fine laminations and/or true marine varves could rework fine grain-size sediment. The widespread presence of Tertiary diatoms may be proof of such reworking (Lloyd Burckle, personal communication, 1999). A detailed investigation of the recognized lithofacies should be addressed to gain a better understanding of deep-water processes responsible for the finely laminated layers. By considering results from table 3, the interpretation of the three r values could offer useful elements to recognize in advance similarities and differences among

apparently similar X-ray lithofacies. However, the use of Correlation Coefficient (r) as a quite sensitive, analytical tool for tracking environmental changes in the factors affecting the physical features, should be validated by further sediment analyses because of its still empirical nature.

Finally, such changes are expected to occur in the petrology of IRD layers of ANTA95-89C and more petrologic-geochemical (*e.g.* radiogenic isotope) investigations are needed, as they are the only realistic tools for tracing diamicton provenance.

ACKOWLEDGEMENTS - Financial support came from the Italian *Programma Nazionale di Ricerche in Antartide* (PNRA). The authors wish to thank Lloyd Burckle, Sidney Hemming and Alex Piotrowski (Lamont-Doherty Earth Observatory) for their valuable suggestions and critical review of the paper. Special thanks also to Mariangela Ravaioli (IGM-CNR, Bologna) for the magnetic susceptibility data and to Furio Finocchiaro (DiSGAM-University of Trieste), who made the measurement and for useful discussion. The staff of X-ray Laboratory of WÄRTSILÄ NSD Italia S.p.A. Trieste is gratefully acknowledged.

REFERENCES

Anderson J.B., Shipp S., Bartek L.R. & Reid D.E., 1992. Evidence for a grounded Ice sheet on the Ross Sea continental shelf during the late Pleistocene and preliminary paleodrainage reconstruction. *Antarctic Research Series, American Geophysical Union*, Washington, DC., **57**, 39-62.

Andrews J.T. & Tedesco K., 1992. Detrital carbonate-rich sediments, northwestern Labrador Sea: Implications for ice-sheet dynamics and iceberg rafting (Heinrich) events in the North Atlantic. *Geology*, **20**, 1087-1090.

Backer S.R & Friedman G.M., 1969. A non-destructive core analysis technique using X-rays. *Journal Sedimentary Petrology*, **39**(4), 1371-1383.

Bentley C.R. & Jezek K.C., 1981. RISS, RISP, and RIGGS: Post-IGY glaciological investigations of the Ross Ice shelf in the U.S. Programme. *Journal Royal Society of New Zealand*, **11**, 355-372.

Blomendal J., King J.W., Hall F.R. & Doh S.J., 1992. Rock magnetism of late Neogene and Pleistocene deep-sea Sediments: Relationship to sediment source, diagenetic processes, and sediment lithology. *Journal of Geophysical Research*, **97**, 4361-4375.

Bond G., Broecker W., Johnson S., McManus J., Labeyrie L., Jouzel J. & Bonani G., 1993. Correlation between climate records from North Atlantic sediments and Greenland ice. *Nature*, **365**, 143-147.

Bouma A.H., 1964. Notes on X-ray interpretation of marine sediments. *Marine Geology*, **2**, 278-309.

Brambati A., Fanzutti G.P., Finocchiaro F., Melis R., Frignani M., Ravaioli M., & Setti M., 1997. Paleoenvironmental record in core ANTA91-30 9 (Drygalski Basin, Ross Sea, Antarctica). In: *Geology and Seismic Stratigraphy of the Antarctic margins, part. 2. Antarctic Res. Series, 71, American Geophysical Union*, Washington, D.C., 137-151.

Domak E.W. & Harris P.T., 1998. A new depositional model for ice shelves, based upon sediment cores from the Ross Sea and the Mac. Robertson shelf, Antarctica. *Annals of Glaciology*, **27**, 281-284.

Fillon H., 1972. Evidence from the Ross Sea for widespread submarine erosion. *Nature Physical. Science.* **238**, 40-42.

Grobe H., Huybrechts P., & Fütterer D.K., 1992. Late Quaternary record of sea-level changes in the Antarctic. *Geologische Rundschau*, **82**, 263-275.

Gunn D.E. & Best A.I., 1998. A mew automated nondestructive system for high resolution multi-sensor core logging of open sediment cores. *Geo-Marine Letters*, **18**, 70-77.

Gwiadza R.H., Hemming S.R. & Broecker W.S., 1996. Provenance of icebergs during Heinrich event 3 and the contrast to their sources during other Heinrich episodes. *Paleoceanography*, 11(**4**), 371-378.

Heinrich H., 1988. Origin and consequences of cyclic ice rafting in the Northeast Atlantic Ocean during the past 130,000 years. *Quaternary Research*, **29**, 142-152.

Hemming S.R., Broecker W.S., Sharp W.D., Bond G.C., Gwiazda R.H., McManus J.F., Klas, M. & Hajdas I., 1998. Provenance of Heinrich layers in core V28-82, northeastern Atlantic: $^{40}Ar/^{39}Ar$ ages of ice-rafted hornblende, Pb isotopes in feldspar grains, and Nd-Sr-Pb isotopes in the fine sediment fraction. *Earth and Planetary Science Letter*, **164**, 317-333.

Hughes T.J., 1977. West Antarctic ice streams. *Reviews of Geophysics*, **15**, 1-46.

Keany J., Ledbetter M., Watkins N. & Huang T.C., 1976. Diachronus deposition of ice-rafted debris in sub-Antarctic deep sea-sediments, *Geological Society American Bulletin, 87, 873-882.*

Kellogg T.B. & Kellogg D.E., 1988. Antarctic cryogenic sediments: biotic and inorganic facies of ice shelf and marine-based ice sheet environment. *Palaeogeography Palaeoclimatology Palaeoecology*, **67**, 51-74.

Leventer A. & Stevens L., 1996. Analysis of laminated Antarctic marine sediments. *Antarctic Journal of the U.S.* – review, 31(**2**), 94-96.

Leventer A., Dunbar, R.B. & De-Master, D.J., 1993. Diatom evidence for late Holocene climatic events in Granite Harbor, Antarctica. *Paleoceanography*, **8**, 373-386.

Moskowitz B.M., Frankel R.B. & Bazylinski D.A. 1993. Rock magnetic criteria for the detection of biogenic magnetite. *Earth Planetary. Science. Letter.*, **120**, 283-300.

Niessen F. & Jarrard R.D., 1998. Velocity and Porosity from CRP-1 Drillhole, Ross Antarctica. *Terra Antarctica,* 5(**3**), 311-318.

Niessen F., Jarrard R.D. & Bucker C., 1998. Log Based Physical Properties of the CRP-1 Core, Ross Sea, Antarctica. *Terra Antarctica,* 5(**3**), 299-310.

Nishimura A., Nakasone T., Hiramatsu C. & Tanahashi M., 1998. Late Quaternary paleoenvironment of the Ross Sea continental shelf, Antarctica. *Annals of Glaciology*, **27**, 275-280.

Oppenheimer M., 1998. Global warming and the stability of the West Antarctic Ice Sheet. *Nature,* **393**, 325-332.

Osterman L.E. & Kellogg, T.B., 1979. Recent benthonic foraminiferal distributions from the Ross Sea, Antarctica: Relation to ecologic and Oceanographic conditions. *Journal Foraminiferal Research.* 9(**3**), 250-269.

Pudsey C.J. & Camerlenghi A., 1998. Glacial-interglacial deposition on a sediment drift on the Pacific margin of the Antarctic Peninsula. *Antarctic Science*, 10(**3**), 286-308.

Rack F. R., Heise E. A. & Stein R., 1995. Magnetic Susceptibility and Physical properties of sediment cores from Site 893, Santa Barbara Basin: Records of sediment diagenesis or of palaeoclimatic and palaeoceanographic change? *Proceedings ODP, Science Results,* **146**,145-168.

SCAR Antarctic Seismic Data Library System, 1983. Ross Sea area, cruise 1987, organization: Sevmorgeolgia (Russia), SDLS-13.

Thomas R.H. & Bentley C.R., 1978. A model for the Holocene retreat of the West Antarctic Ice Sheet. *Quaternary Research,* **10**, 150-170.

Truesdale R.S. & Kellogg T.B., 1979. Ross Sea diatoms: modern assemblage distributions and their relationship to ecologic, oceanographic, and sedimentary conditions. *Marine Micropaleontology*, **4**, 13-31.

Warnke D.A., 1970. Glacial erosion, ice rafting, and glacial marine sediments: Antarctica and the Southern Oceans. *American Journal of Science,* 269, 276-294.

Watkins N.D., Keany J., Ledbetter M.T. & Huang T.C., 1974. Antarctic glacial history from analyses of ice-rafted deposits in marine Sediments: New model and initial test. *Science,* 186, 533-536.

Watkins N.D., 1972. Examination of the Eltanin Dredged Rocks from High latitudes of the South Pacific Ocean. *Antarctic Geology and Geophysics*, IUGS paper, Oslo, 61-70.